Letter Vol. 48, No. 18 / 15 September 2023 / Optics Letters 4825

Optics Letters

Long-range distributed vibration sensing using phase-sensitive forward optical transmission

George Y. Chen,[1,2] Kuan Liu,[1,2] Xing Rao,[1,2] Yuhang Wang,[1,2] Mamoona Khalid,[3] Jun He,[1,2] and Yiping Wang[1,2,*]

[1] Key Laboratory of Optoelectronic Devices and Systems of Ministry of Education and Guangdong Province, College of Physics and Optoelectronic Engineering, Shenzhen University, Shenzhen 518060, China
[2] Shenzhen Key Laboratory of Photonic Devices and Sensing Systems for Internet of Things, Guangdong and Hong Kong Joint Research Centre for Optical Fibre Sensors, Shenzhen University, Shenzhen 518060, China
[3] Photonics and Communications Laboratory, Electrical Engineering Department, University of Engineering and Technology, Taxila, Pakistan
*ypwang@szu.edu.cn

Received 18 July 2023; revised 8 August 2023; accepted 8 August 2023; posted 10 August 2023; published 8 September 2023

Long-range vibration sensing is an important tool for real-time structural health monitoring. A new, to the best of our knowledge, design of a distributed fiber-optic vibration sensor is introduced and experimentally demonstrated in this study. The proposed system utilizes the transmission of light in the forward direction for sensing, and a self-interference method for laser source simplification. To extract vibration information from phase modulation of light, two Mach–Zehnder interferometers (MZIs) are employed with a 3 × 3 coupler-based differential cross multiplication algorithm for phase calculation. A folded double-ended detection configuration allows the time-of-flight difference via cross correlation (CC) to provide vibration positioning. Experimental results demonstrate a sensing range of up to ~80 km without optical amplification, accompanied by a position accuracy of 336 m.

https://doi.org/10.1364/OL.500587

Distributed fiber-optic acoustic/vibration sensors are widely used along railways, dams, and mountains, and in coal and oil extraction sites. Within the frequency range of several hundred hertz, vibration sensing technology can be widely applied in railway transportation, such as for real-time monitoring of railway line vibration. Such long-range sensing systems are able to effectively monitor the structural health of both natural and man-made structures. Through continuous monitoring, it is possible to rapidly identify irregularities and effectively mitigate potential accidents.

Optical fiber-based sensors are gaining popularity due to the many advantages offered by optical fibers compared to traditional electrical sensors, such as sensitivity, resilience to electromagnetic interference (EMI), and resistance to heat. Distributed fiber-optic sensors [1] possess advantages such as high sensitivity, wide dynamic range, reliability, spatially resolved information-gathering ability, and resistance to EMI. Therefore, they are one of the few suitable technologies for monitoring hazardous and remote environments on land and on the seabed. Optical frequency domain reflectometry (OFDR) [2,3] is designed for short sensing range and high spatial resolution. Polarization optical time-domain reflectometry (P-OTDR) [4] can be used for vibration detection, with the advantage of low temperature cross-sensitivity. Phase-sensitive optical time-domain reflectometry [5–9] (φ-OTDR, also known as distributed acoustic sensing or DAS), is the widely used distributed fiber-optic vibration sensing technology that relies on detection of Rayleigh backscattered light. DAS is designed for medium sensing ranges and medium spatial resolution, with a typical maximum range of 40–50 km without deploying optical amplifiers. Sensing systems with much longer sensing distances are highly sought after as they can significantly reduce the resources and maintenance required by avoiding the need for enroute signal boosting.

Forward transmission sensing is an emerging distributed sensing method that is fundamentally different from optical reflectometry methods such as φ-OTDR. This is because the propagation direction of optical signals is the same as that of optical communication. The benefits typically include simpler installation and maintenance in both remote and hazardous environments. Existing designs of such forward transmission sensors are typically based on classic Sagnac loops [10] or Mach–Zehnder interferometers (MZIs) [11,12]. Moreover, hybrid sensor designs employing φ-OTDR and Mach–Zehnder interferometry were also reported by Zhao *et al.* in Ref. [13]. However, existing designs rely on expensive highly coherent laser sources and complex system layouts.

To address these issues, we proposed a new forward transmission fiber-optic acoustic/vibration sensor based on a dual-ended self-interference MZI demodulation that can achieve a sensing range of at least 80 km without an optical amplifier. The proposed design applies signal processing techniques to extract the optical phase in order to analyze distance-resolved vibration signals, along with vibration amplitude and frequency.

There are multiple advantages of forward transmission sensing. These include: (a) higher SNR (optical power is several orders of magnitude higher than backscattering light), unaffected by Rayleigh backscattering noise; (b) fewer nonlinear effects (continuous wave light); (c) longer sensing distances to

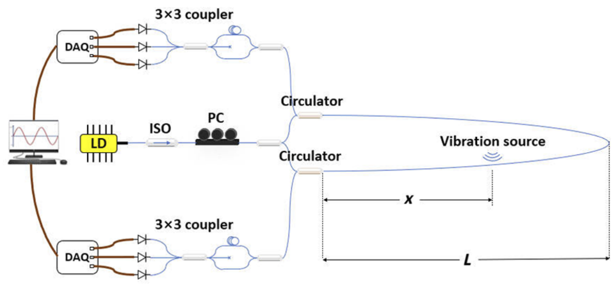

Fig. 1. Schematic of distributed sensing system. LD: laser diode, PC: polarization controller, and DAQ: data acquisition module.

avoid optical amplifiers (easier installation and maintenance); (d) vibration positioning and spatial resolution to mitigate dispersion effects (allowing individual optimization without trade-offs); (e) spatial resolution not directly related to the sensing range (allowing individual optimization without trade-offs); and (f) unlike double-ended OTDR systems, there is no weak SNR region in the middle of the sensing fiber.

The proposed system shown in Fig. 1 uses a linearly polarized laser source (Thorlabs SFL1550S) at 1550 nm that serves as the probe light, with an optical output power of approximately 5 mW and a linewidth of 50 kHz. Initially, the laser beam passes through an optical isolator (ISO) and a polarization controller (PC) to optimize the state of polarization for improved signal stability. Subsequently, the laser beam is split into two equal-power beams using a 1×2 coupler. These two beams then propagate through another 1×2 coupler, and both are coupled into the same single-mode sensing fiber. Along the sensing fiber, the two beams of light propagate in opposite directions and traverse the entire fiber before entering the phase demodulation stage, which deviates from the conventional approach.

One path in the second 1×2 coupler features a delay line, such that the same optical signal at different time instances interfere at a 3×3 coupler [14], and thus the phase difference is relative to a time/distance-shifted version of itself (gauge length). This elegant approach offers significant advantages, including a substantial reduction in optical fiber consumption, minimal polarization changes at the detection end, and it no longer needs an expensive narrow linewidth laser source for high coherence. It is important to note that the delay fiber lengths are 5 m at both receiving ends. The 3×3 coupler outputs three optical signals (coupler imperfection has negligible impact), which are subsequently converted into electrical signals by a photodetector (Thorlabs DET08CFC/M) with a bandwidth of 5 GHz, and digital signals by an USB oscilloscope (Picoscope 5444D). The sampling rate is 12.5 MHz in order to balance smooth operation and high sampling rate. This conversion allows for further processing and analysis by a LabVIEW program.

When vibration is applied to the sensing fiber, interference occurs at the 3×3 coupler between phase-modulated light and its delayed version. The interference result is divided into three optical signals with a phase difference of 120° between each output [15]:

$$I_n = A + B\cos[\varphi(t) + (n-1) \times \frac{2}{3}\pi], \tag{1}$$

where A is the average light intensity, B is the interference fringe amplitude, $n = 1,2,3$ represent three optical outputs, and $\varphi(t)$ is the phase difference between two positions. The value of $\varphi(t)$ can be demodulated by a differential cross multiplication algorithm, as shown in Fig. 2.

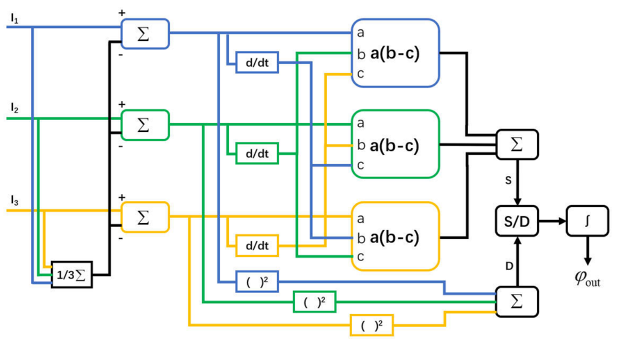

Fig. 2. Differential cross multiplication algorithm for phase derivation.

The difference in arrival time between the two vibration-modulated optical signals can be calculated by the cross correlation (CC) algorithm, which allows the vibration position to be deduced from the time difference. Assuming that a vibration source affects the sensing fiber across a length L, the distance from the perturbation to the system front-end coupler is unknown, denoted by x. The known fiber effective index is n, the light speed in vacuum is c, the time point for detector A to collect the disturbance interference signal in the counterclockwise direction is t_A, and the time point for detector B to collect the disturbance interference signal in the clockwise direction is t_B. The following expressions can be derived:

$$\begin{cases} x = \dfrac{ct_A}{n} \\ 2L - x = \dfrac{ct_B}{n} \end{cases}. \tag{2}$$

The time difference between two interference beams received by each detection end is

$$\Delta t = t_B - t_A = \frac{n(2L-x)}{c} - \frac{nx}{c} = \frac{2n}{c}(L-x). \tag{3}$$

The distance to be determined is denoted by x:

$$x = L - \frac{c\Delta t}{2n}. \tag{4}$$

It can be seen from the above equation that the positioning error d is only related to the measurement error Δt_d of the time delay:

$$d = \frac{c}{2n}(\Delta t - \Delta t_d), \tag{5}$$

where Δt can be determined by applying the CC algorithm to the pair of counter-propagating signals.

Nevertheless, the efficiency of CC is subject to certain limitations. For instance, when the signal frequency is significantly lower than the sampling frequency, the frequency domain spectrum of the signal is concentrated around the fundamental signal frequency. Consequently, the CC outcomes are directly linked to the fundamental frequency and its octave components present in the received signal. With an increasing signal bandwidth, the frequency domain encompasses a greater number of frequency components, thereby causing the CC results to be increasingly influenced by the frequency components present within the bandwidth.

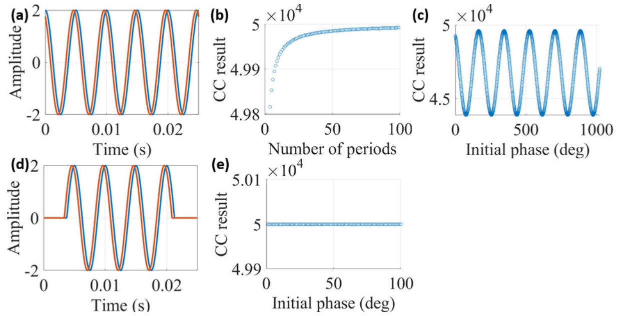

Fig. 3. (a) Simulation of a pair of received signals; (b) CC result as a function of signal periods; (c) CC result changing with the initial phase of the two signals under a fixed phase difference; (d) signal truncation followed by zero padding; (e) CC result of the truncated signal.

For the purpose of improving vibration positioning accuracy, a pre-processing method was used to convert a continuous periodic signal into a finite-length periodic signal. A pair of signals with a fixed time delay were simulated in Fig. 3(a), and CC was performed. The number of periods for each signal was increased while maintaining a constant delay. The calculated CC results are shown in Fig. 3(b), where the result converge toward a steady-state value. However, a large quantity of data points is a significant computational burden. Also, it was found that altering the initial phase of both signals while keeping a constant phase difference would result in an oscillation of the CC result, as depicted in Fig. 3(c). Hence, CC of raw signals has room for improvement. A solution to this problem is to augment the raw signal in order to yield more precise CC outcomes. Therefore, signal processing was performed on the original waveform, starting with identifying two zero-crossing positions and zero padding both sides of the central block of data, as illustrated in Fig. 3(d). Subsequently, CC directly resulted in the true value, as demonstrated in Fig. 3(e).

To test the positioning algorithm, a fiber-coiled piezoelectric transducer (PZT) was placed at ~82 km from one end of the sensing fiber. The demodulated phase signals are shown in Fig. 4(a). A waveform window containing 350,000 data points was used. After the zero padding processing, the truncated signals are shown in Fig. 4(b). It is necessary to ensure that at least five signal periods are retained to reduce positioning errors. Multiple vibration signals of different frequencies are possible, which can be separately analyzed using the Fast Fourier Transform. These signals were subsequently subjected to CC analysis, presented in Fig. 4(c). The spectral shift quality (SSQ) of CC improved from 6.01E-8 to 3.55E-7 after zero padding. The positioning result is illustrated in Fig. 4(d), displaying a deviation of approximately 200 m from the actual value. Under experimental conditions, employing the zero-filling algorithm for the processing of the initial signal led to the generation of CC outcomes that exhibited enhanced accuracy compared to those obtained without any processing (7.68-μs or 795-m positioning error).

The drive voltage and displacement characteristics of the PZT, as well as the estimated strain imposed on the sensing fiber, are shown in Table 1. To evaluate the sensitivity of the system, a stepwise approach was employed where the drive voltage applied to the PZT was incrementally increased and the corresponding demodulated phase recorded. Subsequently, these data

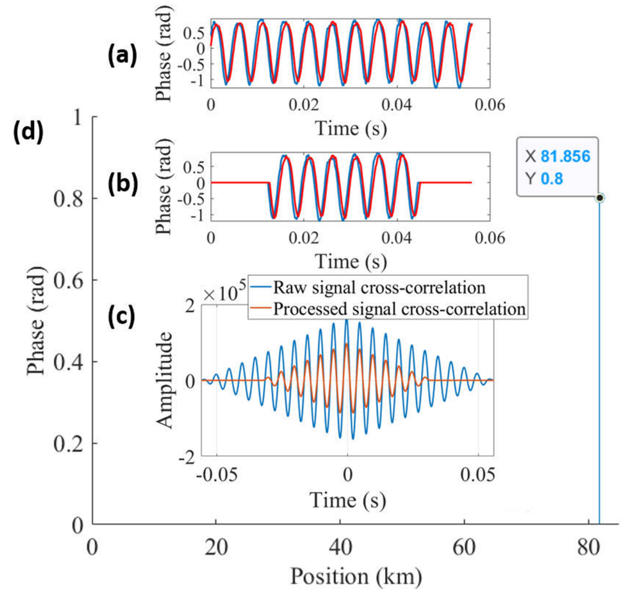

Fig. 4. (a) Original counter-propagating phase signals; (b) phase signals after truncation and zero padding; (c) CC processing; (d) vibration position calculated from time difference.

Table 1. Relationship between PZT Drive Voltage and Strain

Drive Voltage (V)	15	30	45	60	75
Radial displacement (μm)	2.5	5	7.5	10	12.5
Strain (με)	32.0	64.1	96.2	128.2	160.3

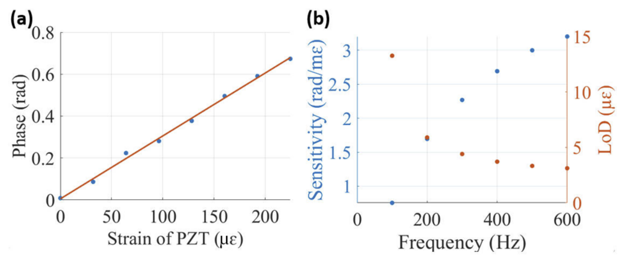

Fig. 5. (a) Relationship between phase and strain, yielding the sensitivity; (b) frequency response of sensitivity and LoD.

points were plotted with a linear fit, as depicted in Fig. 5(a). The gradient deduces the sensitivity as 3.0 mrad/με.

To investigate the frequency response of the sensing system, a series of measurements were carried out at different PZT vibration frequencies, and the corresponding sensitivity and limit of detection (LoD) as a function of vibration frequency were studied. As anticipated, due to the nature of self-interference with a specific delay fiber length (gauge length), it was observed that the sensitivity increased and LoD decreased with higher vibration frequencies (larger phase difference). This observation is supported by the experiment results plotted in Fig. 5(b). The frequency response was characterized within the range of 100 Hz to 600 Hz, limited by the characteristics of the PZT used in the experiment.

The repeatability of positioning accuracy was studied via the collection and analysis of 100 measurements, as shown in Fig. 6(a). The histogram of the measurement results is plotted

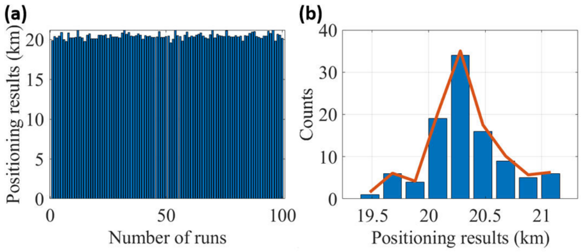

Fig. 6. (a) Vibration positions from 100 measurements; (b) histogram of the measurement results, displaying the probability distribution of Z_m.

in Fig. 6(b), showing the probability distribution of the measured vibration positions, with a root mean square (RMS) error of 336 m, corresponding to the position accuracy. The peak of the Gaussian fitting curve appears at 20.3 km, which is in good agreement with the PZT position.

In conclusion, this study introduces an unconventional distributed fiber-optic acoustic/vibration sensor that utilizes a double-ended forward transmission MZI, offering a promising solution for long-range amplifier-free sensing applications. The experiment results demonstrate the ability to accurately determine vibration amplitude, frequency, and position over long distances. To lower the coherence requirements of the laser source and mitigate cost concerns as well as unwanted phase noise, a self-interference technique is employed. One significant challenge encountered in traditional CC algorithms is the inaccurate estimation of time delay. This issue is effectively resolved through the implementation of truncation and zero padding. The sensitivity was measured to be 3 mrad/με at 500 Hz, the sensing range in excess of 80 km, and the positioning RMS error 336 m. Vibrations were detectable within a frequency range spanning 100 Hz to 600 Hz, limited by the available PZT. Future improvements to the sensor's performance are expected by upgrading the photodetectors to avalanche or single-photon detectors, enabling an extension of the maximum sensing distance. The laser source can be downgraded in terms of broader linewidth (~MHz) to yield the bare minimum coherence length, which helps to reduce phase noise. Additionally, minimizing the position error can be achieved through the adoption of more advanced signal delay algorithms, such as the Time Shifting Deviation method [16].

Disclosures. The authors declare no conflicts of interest.

Data availability. Data underlying the results presented in this paper are not publicly available at this time but may be obtained from the authors upon reasonable request.

REFERENCES

1. X. Liu, B. Jin, Q. Bai, Y. Wang, D. Wang, and Y. Wang, Sensors **16**, 1164 (2016).
2. M. Zhu, D. Leandro, M. López-Amo, and H. Murayma, Opt. Lett. **44**, 1884 (2019).
3. H. Li, Q. Liu, D. Chen, Y. Deng, and Z. He, Opt. Lett. **45**, 563 (2020).
4. Y. Dang, Z. Zhao, X. Wang, R. Liao, and C. Lu, IEEE Access. **7**, 151818 (2019).
5. Z. He and Q. Liu, J. Lightwave Technol. **39**, 3671 (2021).
6. J. Jiang, Z. Wang, Z. Wang, Z. Qiu, C. Liu, and Y. Rao, Opt. Lett. **46**, 685 (2021).
7. Z. Wang, J. Zeng, J. Li, M. Fan, H. Wu, F. Peng, L. Zhang, Y. Zhou, and Y. Rao, Opt. Lett. **39**, 5866 (2014).
8. S. Liu, F. Yu, R. Hong, W. Xu, L. Shao, and F. Wang, Opto-Electron. Adv. **5**, 200078 (2022).
9. F. Peng, H. Wu, X. Jia, Y. Rao, Z. Wang, and Z. Peng, Opt. Express **22**, 13804 (2014).
10. Y. Wang, P. Li, J. Zhang, X. Liu, Q. Bai, D. Wang, M. Zhang, and B. Jin, Measurement **144**, 58 (2019).
11. Z. Zhao, L. Shen, Y. Dang, C. Lu, and M. Tang, Opt. Lett. **46**, 3685 (2021).
12. J. Huang, Y. Chen, Q. Song, H. Peng, P. Zhou, Q. Xiao, and B. Jia, Opt. Express **28**, 24820 (2020).
13. Z. Zhao, M. Tang, L. Wang, N. Guo, H. Tam, and C. Lu, J. Lightwave Technol. **36**, 5764 (2018).
14. S. Spammer, P. Swart, and A. Booysen, Appl. Opt. **35**, 4522 (1996).
15. H. Zhang, M. Zhang, L. Wang, Y. Liao, and D. Wang, Meas. Sci. Technol. **22**, 125203 (2011).
16. Z. Pang, G. Wang, B. Wang, Y. Liao, and D. Wang, J. Lightwave Technol. **40**, 3003 (2022).